

Deformable Mixer Transformer with Gating for Multi-Task Learning of Dense Prediction

Yangyang Xu¹ · Yibo Yang² · Bernard Ghanem² · Lefei Zhang¹

Received: date / Accepted: date

Abstract Convolution neural networks (CNNs) and Transformers have their own advantages and both have been widely used for dense prediction in multi-task learning (MTL). Most of the current studies on MTL solely rely on CNN or Transformer. In this work, we present a novel MTL model by combining both merits of deformable CNN and query-based Transformer with shared gating for multi-task learning of dense prediction. This combination may offer a simple and efficient solution owing to its powerful and flexible task-specific learning and advantages of lower cost, less complexity and smaller parameters than the traditional MTL methods. We introduce deformable mixer Transformer with gating (DeMTG), a simple and effective encoder-decoder architecture up-to-date that incorporates the convolution and attention mechanism in a unified network for MTL. It is exquisitely designed to use advantages of each block, and provide deformable and comprehensive features for all tasks from local and global perspective. First, the deformable mixer encoder contains two types of operators: the channel-aware mixing operator leveraged to allow communication among different channels, and the spatial-aware deformable operator with deformable convolution applied to efficiently sample more informative spatial locations. Second, the task-aware gating transformer decoder is used to perform the task-specific predictions, in which task interaction block integrated with self-attention is applied to capture task interaction features, and the task query block

integrated with gating attention is leveraged to select corresponding task-specific features. Further, the experiment results demonstrate that the proposed DeMTG uses fewer GFLOPs and significantly outperforms current Transformer-based and CNN-based competitive models on a variety of metrics on three dense prediction datasets (*i.e.*, NYUD-v2, PASCAL-Context, and Cityscapes). For example, by using Swin-L as a backbone, our method achieves 57.55 mIoU segmentation on NYUD-v2, outperforming the best existing method by +3.99 mIoU. Our code and models are available at <https://github.com/yangyangxu0/DeMTG>.

Keywords Scene Understanding, Multi-Task Learning, Dense Prediction, CNNs, Transformers

1 Introduction

Human visual system possesses remarkable capabilities, enabling it to perform a multitude of tasks within a single visual scene, including classification, segmentation, and recognition. Consequently, multi-task learning (MTL) has become a prominent area of research in the field of computer vision. Our objective is to develop an advanced vision model capable of simultaneously performing multiple tasks across diverse visual scenarios, with a strong emphasis on efficiency. As shown in Figure 2, in this paper, we aim to develop an efficient and powerful vision model to learn multiple tasks, including semantic segmentation, human parts segmentation, depth estimation, boundary detection, saliency estimation, and normal estimation simultaneously.

Recently, existing works (Liu et al., 2019; Vandenhende et al., 2020; Ghiasi et al., 2021; Bruggemann et al., 2021; Xu et al., 2022b; Bhattacharjee et al.,

✉ Lefei Zhang (*Corresponding Author.*)
E-mail: zhanglefei@whu.edu.cn

¹ School of Computer Science, Wuhan University, Wuhan, China

² King Abdullah University of Science and Technology, Jeddah, Saudi Arabia.

2022; Ye and Xu, 2022) have achieved significant advancements through CNN and Transformer technologies for MTL of dense prediction. CNN-based MTL models are carefully proposed to capture local information and then achieve promising performance on the multi-task dense prediction task. Cross-stitch (Misra et al., 2016) introduces a sharing unit that serves as a combination of the activation to learn an optimal combination of shared and task-specific representations. Some works (Bruggemann et al., 2021; Vandenhende et al., 2020) develop a distillation scheme to enhance the expressiveness of the cross-task and global information passing via enlarging the receptive field and stacking multiple convolutional layers. Transformer-based MTL models (Bhattacharjee et al., 2022; Xu et al., 2022b,a) utilize the efficient self-attention mechanism (Vaswani et al., 2017) for efficient modeling of global and task interactions.

We, in particular, identify three challenges. First, although CNN-based MTL models have been proven effective for MTL in convolutional methods (Gao et al., 2019; Vandenhende et al., 2020; Ghiasi et al., 2021), which better capture the multiple task context in a local field, they suffer from a lack of global modeling and task interaction. These CNN-based MTL methods usually focus on modeling locality naturally, thus lacking the capability to model long-range dependency. Recently, there have been a few attempts (Bruggemann et al., 2021) to introduce the global and local context distillation by using scaled dot-product attention. However, these distillation pipelines still severely limit the global dependencies and are complex.

Second, existing Transformer-based models (Bhattacharjee et al., 2022; Ye and Xu, 2022) excel at modeling the global dependency of different tasks and better focus on global task interactions in MTL. However, these plain self-attention mechanisms ignore task awareness of local structures and introduce huge computation costs. Specifically, it only focuses on capturing long-range dependencies without task-aware local structures during self-attention processing. The queries, keys, and values involve heavy calculation during the interaction, especially for high-resolution inputs.

Third, although our DeMT method can capture the local and global features, it can hardly select task-relevant features effectively in the corresponding task. As a result, the origin DeMT learning by query-based transformer may only focus on the task features and ignore the task-relevant selection, which might be useful for each task.

Recent works (Liu et al., 2021c; Chen et al., 2023) demonstrate that locality is a reasonable compensation for global dependency. However, the potential benefits

of integrating CNN and Transformer in MTL have yet to be fully explored. These challenges motivate us to explore using CNNs and Transformers to capture local and global information with effective mechanisms in MTL in this paper. To address the challenges, we introduce the **Deformable Mixer Transformers with Gating** (DeMTG): a simple and effective method for multi-task dense prediction based on combining both merits of deformable CNN and query-based Transformer. To avoid the naive combination of CNN and Transformer, we originally design the deformable mixer encoder and task-aware gating Transformer decoder.

Specifically, the deformable mixer encoder of our DeMTG consists of channel-aware mixing and spatial-aware deformable convolution. Motivated by the success of deformable convolutional networks (Zhu et al., 2019) in vision tasks, our deformable mixer encoder learns different deformed features for each task based on more efficient sampling spatial locations and channel location mixing (*i.e.*, deformed feature). It learns multiple deformed features highlighting more informative regions with respect to the different tasks. The task-aware gating transformer decoder of our DeMTG consists of task interaction block and task query gating blocks. In the task-aware gating transformer decoder, the multiple deformed features are fused and fed into our task interaction block. We use the fused feature to generate task-interacted features via a multi-head self-attention for model task interactions. Current Transformer-based studies for MTL use regular query tokens. In contrast, we use deformed features as query tokens via attention with gating, which increases the task awareness for the final representation output by the Task-aware Gating Transformer Decoder. Thus, we use deformed features directly as *query* tokens to focus on the task awareness of each task. We expect the set of candidate *key/value* to be from task-interacted features. Then, our task query gating block uses the deformed features and task-interacted features as input and generates the selected task awareness features.

In this way, our deformable mixer encoder selects more valuable regions as deformed features to alleviate the lack of global modeling in CNN. The task-aware gating transformer decoder performs the task interactions by self-attention and enhances task awareness via a query-based Transformer with a shared gating. This design both reduces computational costs and focuses on task awareness features.

We conduct extensive experiments on three dense prediction datasets. Our DeMTG approach consistently outperforms the state-of-the-art methods on a variety of metrics (see Figure 1). We also perform extensive ablation studies to verify the effectiveness and show the

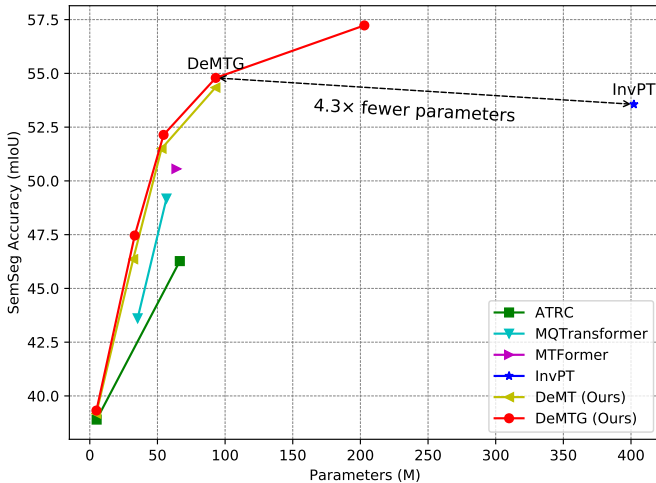


Fig. 1: Accuracy/Parameters trade-off on NYUD-v2. Our DeMTG can outperform existing MTL methods by a large margin on semantic segmentation (SemSeg) accuracy.

significant properties of our DeMTG method. The main contributions of this paper are summarized as follows:

1) We propose a simple and effective DeMTG method for MTL of dense prediction via combining both merits of CNN and Transformer. Most importantly, our approach not only alleviates the lack of global modeling in MTL models using CNNs but also avoids the lack of task awareness in MTL models using Transformers.

2) We introduce a deformable mixer transformer with gating (DeMTG) model, which consists of the deformable mixer encoder (Section 3.3) and task-aware gating transformer decoder (Section 3.4). The deformable mixer encoder produces the deformed features. The task-aware gating transformer decoder uses the deformed features to model task interaction via self-attention and focuses on the task awareness features via a query-based transformer.

3) A novel shared gating layer across all tasks is introduced to perform feature selection transformation, *i.e.*, emphasizing informative features and allowing only the task-relevant information to pass further through the task-aware gating transformer decoder, thus leading to high-quality task-aware outputs.

4) The extensive experiments are conducted on NYUD-v2 (Silberman et al., 2012), PASCAL-Context (Chen et al., 2014), and Cityscapes (Cordts et al., 2016). The visualization results show the efficacy of our model. DeMTG’s strong performance on MTL can demonstrate the benefits of combining the deformable CNN and query-based Transformer. As shown in Figure 1, it outperforms all state-of-the-art methods by a large margin on SemSeg.

This journal paper extends our preliminary work (Xu et al., 2023) in a number of aspects. **First**, we intro-

duce a novel simplified gating mechanism into the original task-aware gating transformer decoder to selectively gather contexts for each query token based on its content. **Second**, by designing a shared spatial gating layer, we further apply shared spatial gating to each task-specific feature in the task query gating block. **Third**, we add more exploration studies on the different aspects of the DeMTG framework and more experimental investigation on one new dataset (Cityscapes (Cordts et al., 2016)). **Finally**, based on the proposed DeMTG, we present an effective and efficient MTL model and give a detailed analysis of different components of our method to highlight the essential ingredients.

2 Related Work

2.1 Multi-Task Learning (MTL)

Multi-task learning (MTL) has become an increasingly popular area of research in recent years, with many works proposing new methods and architectures to tackle the challenges of learning multiple tasks simultaneously. MTL has undergone significant evolution with the advancements in CNNs and Vision Transformers. MTL tasks are primarily distributed in two aspects: the development of innovative model architectures (Brugemann et al., 2021) and the optimization of task loss weighting (Bhattacharjee et al., 2022). In the vision domain, the core idea of MTL is to use a single model to predict semantic segmentation, human parts segmentation, depth, surface normal, boundary, *etc.*, which is an interesting topic. Recent works propose novel architectures that learn shared representation to capture both task-specific and shared information, enhancing overall performance. MuST (Ghiasi et al., 2021) model uses the knowledge in independent specialized teacher models to train a general model for creating general visual representations. Several recent MTL frameworks follow different technologies: (Gao et al., 2019) and (Vandenhende et al., 2020) are convolutional neural network (CNN)-based MTL models, (Brugemann et al., 2021) is Neural Architecture Search (NAS)-based model and (Bhattacharjee et al., 2022; Xu et al., 2022b,a; Ye and Xu, 2022) are Transformer-based models.

(Vandenhende et al., 2021) states that the MTL structures in vision tasks can be summarized into two categories: encoder-focused and decoder-focused architectures. Some encoder-focused works (Kendall et al., 2018; Chen et al., 2018) rely on a shared encoder to learn a general visual feature. The shared encoder extracts features that are subsequently fed into task-specific heads, which perform dense predictions for each individual task. Decoder-focused works (Gao et al., 2019;

Zhang et al., 2019; Bruggemann et al., 2021; Li et al., 2022a) use a shared backbone network to extract a shared feature for each task. Then, the designed task-specific modules perform the interactions to capture valuable information from the cross-task. In the proposed method, MTI-Net (Vandenhende et al., 2020), explicitly models task interactions at multiple scales, propagates distilled task information from lower to higher scales, and aggregates refined task features from all scales to generate the final per-task predictions. ATRC (Bruggemann et al., 2021) introduces the adaptive module that automatically selects the most efficient attention-based context for refining task predictions in a multi-task environment. (Li et al., 2022a) highlights that cross-task relations are crucial to learning multi-task dense prediction problems via learning relations between task pairs in joint latent spaces.

With a series of Vision Transformer (Dosovitskiy et al., 2021) successes, the exploitation of advanced computing has enabled multi-task learning to receive significant performance improvements. Specifically, MTFormer (Xu et al., 2022a) and InvPT (Ye and Xu, 2022) use a self-attention mechanism with a strong backbone to boost the MTL of dense prediction performance. Unlike Transformer-based MTL methods, MQTranformer (Xu et al., 2022b) leverages the multi-task queries to perform the task interactions and transfer the task-specific knowledge. However, these MTL methods primarily focus on the shared feature, which is hard to disentangle the task-specific features.

2.2 Deformable CNNs and Vision Transformers.

Deformable CNNs. CNNs have achieved milestone contributions in many domains. Deformable ConvNets (Dai et al., 2017; Zhu et al., 2019) harness the enriched modeling capability of CNNs (Yang et al., 2020) via deformable convolution and deformable spatial locations. Deformable ConvNets is the first to achieve competitive results in vision tasks (*e.g.*, object detection and semantic segmentation, *etc.*) using deformable convolution. Deformable convolution can attend to flexible spatial locations conditioned with offset on input images. Thus, the deformable concept is introduced into Transformer via deformed points. Deformable transformers (Zhu et al., 2021; Xia et al., 2022) attend to a small set of crucial sampling points around a reference and capture more informative features. (Xia et al., 2022) develop a deformable self-attention module to address concerns with the use of dense and sparse attention in vision tasks and introduces the deformable attention Transformer as a general backbone model for both image classification and dense prediction tasks.

CNNs are widely used for MTL, and recent works have proposed various CNN-based architectures to learn shared features across tasks. UberNet (Kokkinos, 2017) is proposed to train in an end-to-end manner a unified CNN architecture to solve multiple vision tasks. NDDR-CNN (Gao et al., 2019) introduces a CNN structure, neural discriminative dimensionality reduction, for multi-task learning, which enables automatic feature fusing at every layer and is formulated by combining existing CNN components in a novel way with clear mathematical interpretability. In addition, MTI-Net (Vandenhende et al., 2020) proposes MTL architecture for multi-task learning, which models task interactions at multiple scales through a multi-scale multi-modal distillation unit, feature propagation module, and feature aggregation unit to produce refined task features and improve performance on dense prediction tasks. Previous CNN-based MTL methods utilize plain convolution to capture the task’s local information from the input feature. However, these methods may not exploit the global information available for each task. In our method, we improve the transformer by replacing the self-attention variables (*i.e.*, *query*, *key*, and *value*) with the deformable features as query, key, and value tokens. Our method performs deformable convolution over the input feature, which contains informative features for each task.

Vision Transformers. Transformers and attention (Vaswani et al., 2017) mechanisms have shown great success in natural language processing tasks and have also been applied to computer vision tasks such as object detection, classification and segmentation. Transformer structures have also produced impressive results in computer vision and tend to replace CNN progressively. Transformer architectures are applied in vision tasks by splitting an image into a sequence of visual patches. ViT (Dosovitskiy et al., 2021) is the first work to derive from the self-attention mechanism for computer vision tasks and demonstrates superior performance to modern CNNs. Recently, there has been growing interest in applying transformer-based architectures for dense prediction in computer vision. More Transformer-based approaches (Carion et al., 2020; Liu et al., 2021c; Ranftl et al., 2021; Wang et al., 2021; Lan et al., 2022; Ru et al., 2022) have been introduced by improving the attention mechanism for dense prediction tasks. Different from the original designs in (Vaswani et al., 2017; Dosovitskiy et al., 2021), some vision Transformers usually employ a hierarchical architecture and change the global self-attention among all patches to local self-attention to develop efficient attention mechanisms. These efficient attention mechanisms include windowed attention (Dong et al., 2022; Liu et al., 2021c), global tokens (Jaegle et al., 2021), gated attention (Yang et al.,

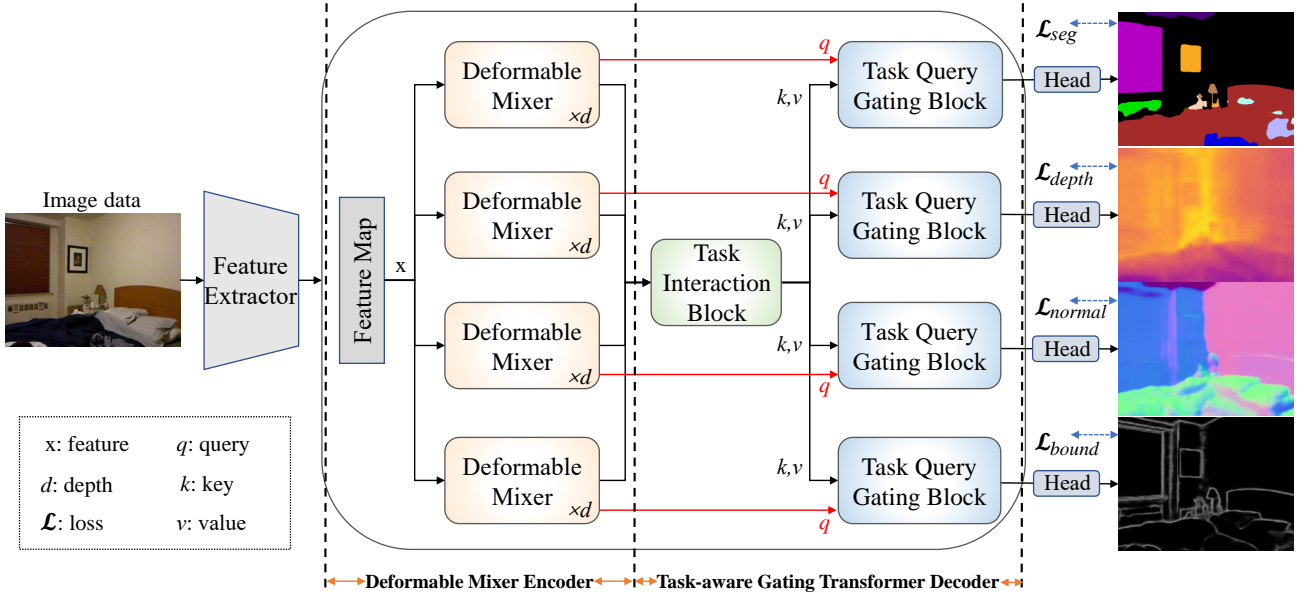


Fig. 2: An overview of our model jointly handles multiple tasks with a unified encoder-decoder architecture. Our DeMTG model consists of the deformable mixer encoder and task-aware gating transformer decoder. The core blocks of our DeMTG are (a) the deformable mixer (DM) that generates task-relevant deformable features, (b) the task interaction block that performs the interaction, and (c) the task query gating block that can obtain the task-aware features through selection. The depth d is the number of repetitions of the Deformable Mixer (ablation on the d in Table 5(b)).

2022; Fei, 2022) and deformable attention (Zhu et al., 2021; Xia et al., 2022). Recently, these works are also extended to the MTL domain to learn good representations for multiple tasks of dense predictions. In MTL, transformer-based architectures have been proposed to learn a shared feature representation across tasks via self-attention. Mult (Bhattacharjee et al., 2022) uses a shared attention mechanism modeling the dependencies across the tasks to perform MTL of dense prediction. MTFormer (Xu et al., 2022a) designs the shared transformer encoder and shared transformer decoder, and task-specific self-supervised cross-task branches are introduced to obtain final outputs, which increases the MTL performance. In InvPT (Ye and Xu, 2022) work, they use an inverted pyramid multi-task transformer to learn the long-range interaction via plain self-attention in both spatial and all-task contexts on the multi-task feature maps with a gradually increased spatial resolution for the multi-task dense prediction. In contrast, we find the deformed features to focus on the valuable region for different tasks. In addition, we use the query-based transformer with task shared gating block approach for modeling and leverage deformed features as queries in transformer calculations to enhance task-relevant features. These queries can naturally disentangle the task-specific feature from the fused feature. Then the last shared gating mechanism (Fei, 2022). Our approach combines the respective advantages of CNN and Transformer, achieving state-of-the-art per-

formance on NYUD-v2 (Silberman et al., 2012), PASCAL-Context (Chen et al., 2014), and Cityscapes (Cordts et al., 2016) datasets.

3 Approach

3.1 Overall Architecture

We describe the overall framework of our architecture in Figure 2. DeMTG results from a non-shared encoder-decoder procedure: First, we design a deformable mixer encoder to encode task-specific spatial features for each task. Second, the task interaction block and task query gating block are proposed to model the decode of the task interaction information and decode task-specific features via self-attention with gating. In the following section, we describe our multi-task losses.

3.2 Feature Extractor

The feature extractor is employed to aggregate multi-scale features and generate a shared feature map for each task. The utilization of a shared feature map enables the model to leverage information from different scales, thereby enhancing its capacity to perform multiple tasks effectively. As shown in Figure 3, the initial image data $X_{in} \in \mathbb{R}^{H \times W \times 3}$ (3 is image channel)

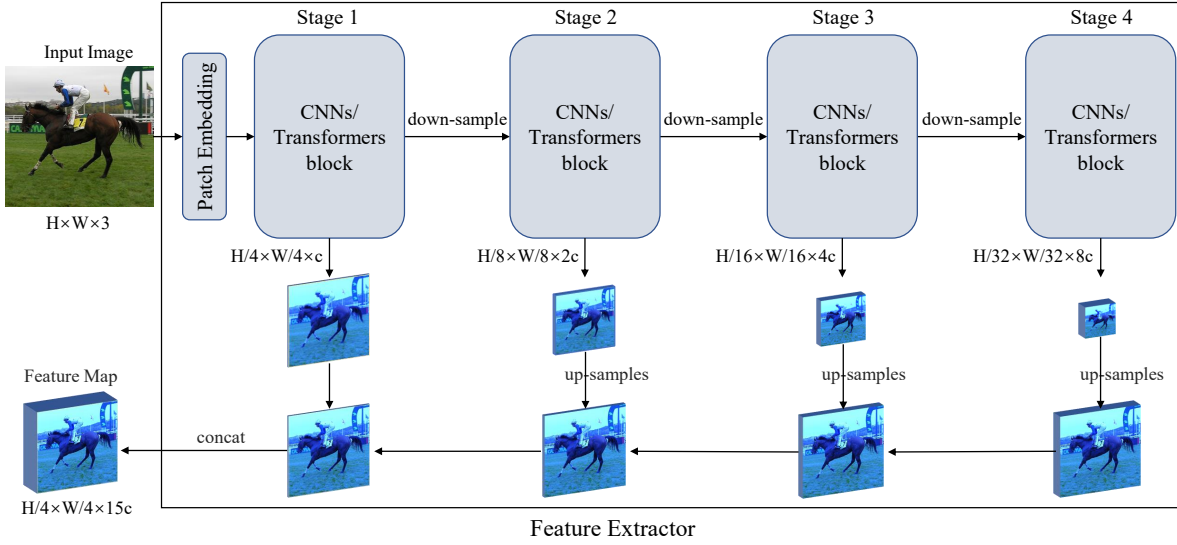


Fig. 3: Illustration of our feature extractor. Our feature extractor can be compatible with two kinds of backbone networks (*i.e.*, Swin-Transformer and HRNet). We conduct the scale number ablation study in Table 5(c). In this figure, we set the feature map channel $15c = C$.

is input to the backbone (CNN-based or Transformer-based), which then generates four stages of image features. The four-stage image features are up-sampled to the same resolution, and then they are concatenated along the channel dimension to obtain an image feature $X \in \mathbb{R}^{\frac{H}{4} \times \frac{W}{4} \times C}$, where H , W , and C are the height, width, and channel of the image feature, respectively. We conduct the ablation study on the four-stage image features in Table 5(c).

3.3 Deformable Mixer Encoder

The motivation. Inspired by the success of the Deformable ConvNets (Zhu et al., 2019) and Deformable DETR methods (Zhu et al., 2021), we propose the deformable mixer encoder that adaptively provides more efficient receptive fields and sampling spatial locations for each task. To achieve this objective, we first introduce a deformable mixer encoder that consists of four operation layers, the linear, a channel-aware mixing, the GELU&BN, and a spatial-aware deformable. The deformable mixing encoder separates the mixing of spatial-aware deformable spatial features and channel-aware location features. As shown in Figure 4, the spatial-aware deformable and channel-aware mixing operators are interleaved to enable interaction of both input feature dimensions ($HW \times C$).

Specifically, we propose a deformable mixer encoder to capture the distinctive receptive regions corresponding to the each individual task. The deformable mixer selectively attends to a small set of crucial sampling

points, represented by learnable offsets. The spatial-aware deformable is capable of effectively modeling spatial context aggregation. Then the spatial-aware deformable, channel-aware mixing, and batch normalization operators are stacked sequentially to form a single deformable mixer. The impact of the deformable mixer stack’s depth on the model is shown in Table 5(b) through an ablation experiment.

The deformable mixer encoder structure is shown in Figure 4. First, a linear layer reduces the channel dimension of the image feature $X \in \mathbb{R}^{\frac{H}{4} \times \frac{W}{4} \times C}$ from C to a smaller dimension C' . The linear layer can be mathematically represented as follows:

$$X = W \cdot \text{Norm}(X), \quad (1)$$

where Norm means LayerNorm function, after the linear layer, we obtain a smaller dimension image feature map $X \in \mathbb{R}^{\frac{H}{4} \times \frac{W}{4} \times C'}$ as the input for the downstream layers.

Channel-aware mixing. Given the input image feature $X_{i,j} \in \mathbb{R}^{\frac{H}{4} \times \frac{W}{4} \times C'}$ obtained from the output of Eq. (1) output, the point (i, j) represents the spatial location in the single channel feature map. The channel-aware mixing facilitates communication between different channels by applying the standard point-wise convolution (where the convolution kernel is 1×1) to mix channel locations. It can be formulated as follows:

$$X_{i,j} = W_1 \cdot X_{i,j} + b, \quad (2)$$

where the W_1 is the point-wise convolution weight. b is a learnable bias. Subsequently, we add GELU activation

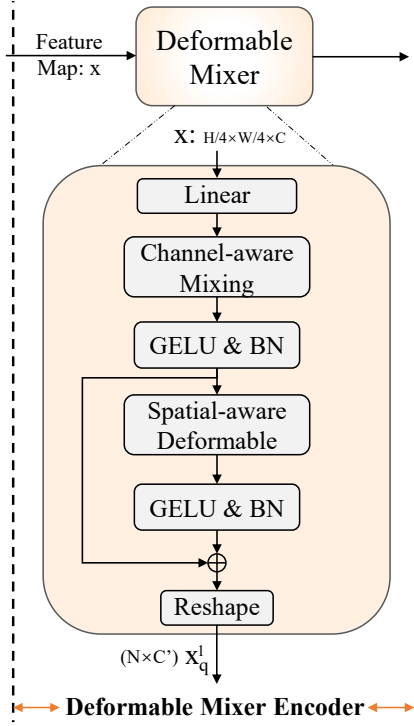


Fig. 4: Illustration of our Deformable Mixer Encoder. For simplicity, we assume there is only one task ($T = 1$) in this figure.

and BatchNorm as well. This operation is calculated as follows:

$$X_{i,j} = \text{BN}(\sigma(X_{i,j})), \quad (3)$$

where $\sigma()$ denotes the activation function.

Spatial-aware deformable. To generate the relative offsets with respect to the reference point, the image feature $X_{i,j}$ obtained from the output of Eq. (3) output, the point (i, j) represents the spatial location. $X_{i,j}$ is fed to the convolution operator to learn the corresponding offsets $\Delta_{(i,j)}$ for all reference points. For each location point (i, j) on the image feature $X_{i,j}$, the spatial deformable can be mathematically represented as follows:

$$D_S(X_{i,j}) = \sum_{C'=0}^{C'-1} W_1 \cdot X((i, j) + \Delta_{(i,j)}, C'), \quad (4)$$

where the W_1 is a deformable weight. The $\Delta_{(i,j)}$ is the learnable offset. The spatial-aware deformable is followed by a GELU activation, BatchNorm, and residual connection:

$$X_{C'} = X_{i,j} + \text{BN}(\sigma(D_S(X_{i,j}))), \quad (5)$$

where $\sigma(\cdot)$ represents the non-linearity function (*i.e.*, GELU), and BN denotes the BatchNorm operation.

We use *Reshape* to denote the rearrangement function. Our feature map $X_{C'}$ can be written as:

$$X_q = \text{Reshape}(X_{C'}), \quad (6)$$

where the *Reshape* is applied to flatten the feature $X_q \in \mathbb{R}^{\frac{H}{4} \times \frac{W}{4} \times C'}$ to a sequence $\mathbb{R}^{N \times C'}$ ($N = \frac{H}{4} \times \frac{W}{4}$). When there are T tasks, the deformable mixer encoder generates a feature set $(X_q^1, X_q^2, \dots, X_q^T)$ (T means task number) as shown in Figure 4. These output task-specific features are learned by a deformable mixer that we refer to as *deformed features*, which we add to the input of the downstream blocks (task interaction block and task query block).

3.4 Task-aware Gating Transformer Decoder

In the task-aware gating transformer decoder, we design the task interaction block and task query gating block (See Figure 5). It is important for MTL to consider task interactions. Thus, we propose a task interaction block to capture the task interactions at every task via a self-attention mechanism. Each task interaction block is composed of two parts, *i.e.*, a multi-head self-attention module (MHSA) and a small Multi-Layer Perceptron (sMLP). The downstream task query block also consists of the MHSA and the sMLP. The difference between the task interaction block and the task query block is that their query features are fundamentally different. The feature is projected into the queries (Q), keys (K), and values (V) of dimension d_k , and self-attention is being computed by the Q , K and V . The self-attention operator is calculated as follows:

$$\text{MHSA}(Q, K, V) = \text{softmax}\left(\frac{QK^T}{\sqrt{d_k}}\right)V, \quad (7)$$

where $Q \in \mathbb{R}^{N \times C'}$, $K \in \mathbb{R}^{N \times C'}$ and $V \in \mathbb{R}^{N \times C'}$ are the query, key and value matrices; $\text{MHSA}(Q, K, V) \in \mathbb{R}^{N \times C'}$.

Task interaction block. As illustrated in Figure 4 (blue box), We first concatenate the deformed features from the deformable mixer encoder output.

$$X_f = \text{Concat}(X_q^1, X_q^2, \dots, X_q^T), \quad (8)$$

where $X_f \in \mathbb{R}^{TN \times C'}$ is the fused feature. The T means task number in $X_q^T \in \mathbb{R}^{N \times C'}$. Then, for efficient task interaction, we construct a self-attention strategy via the fused feature X_f :

$$X'_f = \text{MHSA}(Q, K, V = \text{LN}(X_f), \text{LN}(X_f), \text{LN}(X_f)), \quad (9)$$

$$\hat{X}_f = \text{sMLP}(X'_f), \quad (10)$$

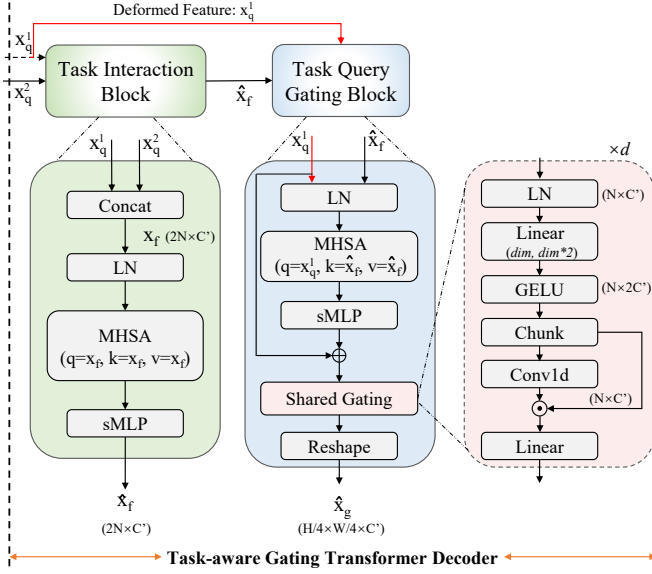


Fig. 5: Illustration of our Task-aware Gating Transformer Decoder. The dim denotes the input dimension. $Conv1d$ denotes 1D convolution operation.

where $\hat{X}_f \in \mathbb{R}^{TN \times C'}$ is the task-interacted feature. LN means LayerNorm function. sMLP consists of a linear layer and a LayerNorm.

Task query gating block. As illustrated in Figure 5 (left), we take the deformed feature X_q as task query and the task-interacted feature \hat{X}_f as key & value to MHSA. The deformed feature is applied as a query in MHSA to decode the task awareness feature from the task-interacted feature for each task prediction. We first apply the LayerNorm in parallel to generate queries Q , keys K and values V :

$$\hat{Q} = \text{LN}(X_q), \quad \hat{K} = \text{LN}(\hat{X}_f), \quad \hat{V} = \text{LN}(\hat{X}_f), \quad (11)$$

where LN is the layer normalization. X_q and \hat{X}_f are the output of the deformable mixer encoder and task interaction block, respectively. Then, the task query block operation using a MHSA is calculated as follows:

$$\hat{X}_q = \text{MHSA}(\hat{Q}, \hat{K}, \hat{V}), \quad (12)$$

$$\hat{X} = X_q + \text{sMLP}(\hat{X}_q), \quad (13)$$

where the residual feature X_q comes from Eq. (5). The task awareness feature $\hat{X} \in \mathbb{R}^{N \times C'}$.

Shared spatial gating layer. As illustrated in Figure 5, we use a shared spatial gating (SSG) layer with a gating mechanism (Dauphin et al., 2017) to improve the information flow through the network. Gating mechanisms control the path through which information flows in the network and have proven to be useful for CNN-based and Transformer-based networks (Dauphin et al.,

2017; Rao et al., 2022; Fei, 2022; Yang et al., 2022). The proposed shared spatial gating is applied to refine each task independently feature through task-relevant selection. The SSG process can be formulated as follows:

$$X_g = \sigma(\text{Linear}(\text{LN}(\hat{X}))), \quad (14)$$

where LN is the layer normalization. $\sigma(\cdot)$ is the non-linearity function (*i.e.*, GELU). We first apply a linear transformation to the incoming task awareness feature (*i.e.*, \hat{X}). After Linear with $\hat{X} \in \mathbb{R}^{N \times C'}$, we obtain the feature $X_g \in \mathbb{R}^{N \times 2C'}$. The X_g is split to $X_g^1 \in \mathbb{R}^{N \times C'}$ and $X_g^2 \in \mathbb{R}^{N \times C'}$ along the channel dimension. Given two features X_g^1 and X_g^2 , the spatial gating is formulated as:

$$X'_g = X_g^1 \odot \text{Conv1d}(\text{LN}(X_g^2)), \quad (15)$$

$$\hat{X}_g = \text{Reshape}(\text{Linear}(X'_g)) \quad (16)$$

where LN is the layer normalization. \odot is the element-wise multiplication between matrices. $Conv1d$ denotes 1D convolution operation. The final spatial gating feature $\hat{X}_g \in \mathbb{R}^{\frac{H}{4} \times \frac{W}{4} \times C'}$ is reshaped from $\mathbb{R}^{N \times C'}$ ($N = \frac{H}{4} \times \frac{W}{4}$) via *Reshape* operation. The SSG controls the task information flow by gating through all the task awareness features, thereby allowing each task to focus on the fine details complementary to the other tasks. Further, we demonstrate the benefits of our shared gating layer by conducting an ablation study in Table 5(a).

3.5 MTL Loss Function

For balancing the loss contribution for each task, we set the weight α_t to decide the loss contribution for the task t . A weighted sum \mathcal{L}_{total} of task-specific losses:

$$\mathcal{L}_{total} = \sum_{t=1}^T \alpha_t \mathcal{L}_t, \quad (17)$$

where the \mathcal{L}_t is a loss function for task t . For fair comparisons, we use α_t and \mathcal{L}_t consistent with ATRC (Brugemann et al., 2021) and MQTransformer (Xu et al., 2022b). Let \mathcal{L}_{total} be the set of total loss of the MTL framework ($\mathcal{L}_{total} = \{\mathcal{L}_{seg}, \mathcal{L}_{partseg}, \mathcal{L}_{sal}, \mathcal{L}_{depth}, \mathcal{L}_{normal}, \mathcal{L}_{bound}\}$). We apply standard cross-entropy loss for SemSeg (\mathcal{L}_{seg}), Human Parts Seg ($\mathcal{L}_{partseg}$) and saliency (\mathcal{L}_{sal}) tasks, which computes the cross entropy loss between input and target. We employ L1Loss for depth (\mathcal{L}_{depth}) and surface normal (\mathcal{L}_{normal}) tasks, which measure the mean absolute error between each element in the input and target. We leverage a binary cross entropy loss for boundary (\mathcal{L}_{bound}) task, which measures binary cross entropy between target and input logits.

4 Experiments

In this section, we conduct extensive experiments on three widely-used dense prediction datasets. We evaluate the performance of our DeMTG method on these datasets and compare it with state-of-the-art MTL methods using various metrics. We perform extensive ablation studies on different components to showcase the improvements contributed by each block. For qualitative evaluation results, see section 4.5 for visualization.

4.1 Setup

Implementation. All the leveraged backbones generate four scales (1/4, 1/8, 1/16, 1/32) features to perform a simple multi-scale aggregation in our feature extractor (See Section 3.2). We train our model using the SGD optimizer with the learning rate to 10^{-3} and weight decay to 5×10^{-4} . We train standard models for 400 epochs on NYUD-v2 dataset and 64 epochs on PASCAL-Context unless otherwise specified. The whole experiments are performed with pre-trained models. We set $\alpha_{seg} = 1.0$, $\alpha_{partseg} = 2.0$, $\alpha_{sal} = 5.0$, $\alpha_{normal} = 10.0$, and $\alpha_{bound} = 50.0$ in Eq. (17) to balance the trade-off between MTL loss. All our experiments are performed on the Pytorch platform with eight A100 SXM4 40GB GPUs.

Datasets. We conduct experiments on three publicly accessible datasets, NYUD-v2 (Silberman et al., 2012), PASCAL-Context (Chen et al., 2014), and Cityscapes (Cordts et al., 2016). NYUD-V2 consists of RGB and Depth frame pairs, of which 795 images are used for training and 654 images are used for testing. NYUD-V2 is commonly utilized for semantic segmentation (‘SemSeg’), depth estimation (‘Depth’), surface normal estimation (‘Normal’), and boundary detection (‘Bound’) tasks, providing dense labels for each image. PASCAL-Context training and validation sets contain 10103 images, while testing contains 9637 images. PASCAL-Context usually is adopted for semantic segmentation (‘SemSeg’), human parts segmentation (‘PartSeg’), saliency estimation (‘Sal’), surface normal estimation (‘Normal’), and boundary detection (‘Bound’) tasks, providing annotations for the whole scene. The Cityscapes dataset focuses on a semantic understanding of urban street scenes and usually is adopted for semantic segmentation (‘SemSeg’) and depth estimation (‘Depth’).

Metrics. We employ six evaluation metrics to compare our model with other prior multi-task models: mean Intersection over Union (mIoU), root mean square error (rmse), mean Error (mErr), absolute error (aErr), optimal dataset scale F-measure (odsF), and maximum F-measure (maxF). These metrics provide comprehensive

assessments of our model’s performance across various tasks and datasets. Since, for multi-task learning, it’s difficult to measure the performance of a model with a single metric; we introduce the average per-task performance drop (Δ_m) metric. The average per-task performance drop (Δ_m) is used to quantify multi-task performance. $\Delta_m = \frac{1}{T} \sum_{i=1}^T (F_{m,i} - F_{s,i}) / F_{s,i} \times 100\%$, where m , s and T mean multi-task model, single task baseline and task numbers. Δ_m : the higher, the better.

Backbones. We evaluate our method using several CNN and Vision Transformer backbones: HRNetV2-W18-small (HRNet18), HRNetV2-W48 (HRNet48) (Sun et al., 2019), Swin-Tiny (Swin-T), Swin-Small (Swin-S), Swin-Base (Swin-B) and Swin-Large (Swin-L) (Liu et al., 2021c).

Baselines. In this paper, we categorize the baseline models into two groups: multi-task learning (MTL) baseline and single-task learning (STL) baseline. These two groups serve as reference points for evaluating the performance of our proposed DeMTG method. Our DeMTG adopts both CNN-based (*i.e.*, HRNet) and Transformer-based (*i.e.*, Swin-Transformer) as backbones. Specifically, we use HRNet18, Swin-T, Swin-S, Swin-B and Swin-L networks as backbones to perform the MTL and STL on NYUD-v2 and PASCAL-Context datasets. We also chose to draw the comparison with the Transformer-based InvPT (Ye and Xu, 2022) and MTFormer (Xu et al., 2022a) methods.

4.2 Comparison with the State-of-the-art

We compare our model with CNN-based and Transformer-based models to show the advantages of our method.

NYUD-v2. We first evaluate our model on the NYUD-v2 (Silberman et al., 2012) dataset, one of the most studied dense prediction datasets. The Comparisons with state-of-the-art models on the NYUD-v2 dataset are shown in Table 1. We follow the evaluation protocol of prior works (Silberman et al., 2012; Xu et al., 2022b). We report results comparison using five different backbones: HRNet18, Swin-T, Swin-S, Swin-B, and Swin-L. We demonstrate simultaneous performance improvements over prior work in having smaller parameters, a similar number of GFLOPs, and better semantic segmentation, depth estimation, surface normal and boundary detection accuracy. For example, a performance comparison between InvPT (Ye and Xu, 2022) and DeMTG proves the effectiveness of our framework. Besides this, DeMTG also consistently outperforms previous state-of-the-art Transformer-based models, such as MQTransformer (Xu et al., 2022b), MTFormer (Xu et al., 2022a), and InvPT (Ye and Xu, 2022). In addition, we also observe that using a Transformer as a backbone model is more promising compared to CNN as the backbone.

Table 1: Comparison of the MTL models with state-of-the-art on NYUD-v2 dataset. The notation ‘↓’: lower is better. The notation ‘↑’: Higher is better. Δ_m denotes the average per-task performance drop. “Params” denotes parameters. Swin-◇ indicates that the specific Swin model is uncertain. ♦ denotes results not reported in InvPT (Ye and Xu, 2022) but from our test.

Model	Backbone	Params (M)	GFLOPs (G)	SemSeg (mIoU)↑	Depth (rmse)↓	Normal (mErr)↓	Bound (odsF)↑	Δ_m [%]↑
single task baseline	HRNet18	16.09	40.93	38.02	0.6104	20.94	76.22	0.00
multi-task baseline	HRNet18	4.52	17.59	36.35	0.6284	21.02	76.36	-1.89
Cross-Stitch(Misra et al., 2016)	HRNet18	4.52	17.59	36.34	0.6290	20.88	76.38	-1.75
Pad-Net(Xu et al., 2018)	HRNet18	5.02	25.18	36.70	0.6264	20.85	76.50	-1.33
PAP(Zhang et al., 2019)	HRNet18	4.54	53.04	36.72	0.6178	20.82	76.42	-0.95
PSD(Ling et al., 2020)	HRNet18	4.71	21.10	36.69	0.6246	20.87	76.42	-1.30
NDDR-CNN(Gao et al., 2019)	HRNet18	4.59	18.68	36.72	0.6288	20.89	76.32	-1.51
MTI-Net(Vandenhende et al., 2020)	HRNet18	12.56	19.14	36.61	0.6270	20.85	76.38	-1.44
ATRC(Bruggemann et al., 2021)	HRNet18	5.06	25.76	38.90	0.6010	20.48	76.34	1.56
DeMT (Ours)	HRNet18	4.76	22.07	39.18	0.5922	20.21	76.40	2.37
DeMTG (Ours)	HRNet18	4.89	28.83	39.32	0.5927	20.17	76.40	2.50
single task baseline	Swin-T	115.08	161.25	42.92	0.6104	20.94	76.22	0.00
multi-task baseline	Swin-T	32.50	96.29	38.78	0.6312	21.05	75.60	-3.74
MQTransformer(Xu et al., 2022b)	Swin-T	35.35	106.02	43.61	0.5979	20.05	76.20	0.31
InvPT (Ye and Xu, 2022)	Swin-T	-	-	44.27	0.5589	20.46	76.10	2.55
DeMT (Ours)	Swin-T	32.07	100.70	46.36	0.5871	20.65	76.90	3.36
DeMTG (Ours)	Swin-T	33.2	125.49	47.20	0.5660	20.15	77.20	5.00
single task baseline	Swin-S	200.33	242.63	48.92	0.5804	20.94	77.20	0.00
multi-task baseline	Swin-S	53.82	116.63	47.90	0.6053	21.17	76.90	-1.96
MQTransformer(Xu et al., 2022b)	Swin-S	56.67	126.37	49.18	0.5785	20.81	77.00	1.59
MTFormer(Xu et al., 2022a)	Swin-◇	64.03	117.73	50.56	0.4830	-	-	4.12
DeMT (Ours)	Swin-S	53.03	121.05	51.50	0.5474	20.02	78.10	4.12
DeMTG (2-task) (Ours)	Swin-S	52.16	96.73	53.59	0.5521	-	-	6.5
DeMTG (Ours)	Swin-S	54.52	145.84	52.23	0.5599	20.05	78.4	4.05
single task baseline	Swin-L	789.96	819.93	56.46	0.508	19.38	78.8	0.00
multi-task baseline	Swin-L	204.96	316.87	54.53	0.532	19.51	78.3	-2.36
InvPT(Ye and Xu, 2022)	Swin-L	-	-	51.76	0.5020	19.39	77.60	-2.22♦
InvPT(Ye and Xu, 2022)	ViT-L	402.1♦	555.57♦	53.56	0.5183	19.04	78.10	-
DeMTG (Ours)	Swin-L	202.92	321.22	57.55	0.5037	19.21	79.00	0.98

Because Transformer-based and CNN-based models use similar Parameters, the former shows higher accuracy in all metrics. Specifically, our DeMTG using Swin-T obtains 47.20 mIoU (SemSeg) accuracy, which is +3.59 (47.20 vs. 43.61) higher than that of MQTransformer with the same Swin-T backbone and similar GFLOPs, while being more parameter efficient. We also find that DeMTG can substantially outperform InvPT (Ye and Xu, 2022) by 2.93 mIoU SemSeg (47.20 vs. 44.27), and we note DeMTG still beats it by +2.45 on Δ_m metric. MuIT shows an improvement with a 13.3% increase in relative performance for semantic segmentation and an 8.54% increase for depth tasks. While our origin DeMT achieves a 14.74% and 9.43% increase compared to MuIT (Bhattacharjee et al., 2022). As shown in Figure 1, our method can outperform the state-of-the-art InvPT, which requires 4.3× more parameters compared to DeMTG. As expected, our DeMTG using Swin-L performs the best, with an almost +5.79 (57.55 vs. 51.76) mIoU improvement in the SemSeg task compared to InvPT (Ye and Xu, 2022). In addition, we report the InvPT using ViT-L (Dosovitskiy et al., 2021)

as backbone performance. We again observe a performance gain than InvPT in SemSeg, Depth, and Bound task in Table 1. The results demonstrate that, even in the different multi-task settings, our DeMTG has the potential to yield further performance gains. Across all task metrics, we find that DeMTG is significantly better than prior works while using fewer parameters. The comparison results show that our model also achieves good performance, evaluating the flexibility of our model. By comparison, our DeMTG achieves new records on the NYUD-v2 (Silberman et al., 2012), which are remarkably superior to previous CNNs and Transformers models in terms of all metrics.

PASCAL-Context. We also evaluate our model on the PASCAL-Context (Chen et al., 2014) dataset, one of the most studied dense prediction datasets. The Comparisons with state-of-the-art models on the PASCAL-Context dataset are shown in Table 2. We perform the experiment on PASCAL-Context with five backbones: HRNet18, Swin-T, Swin-S, Swin-B, and Swin-L. Our model obtains significantly better results when compared with the baseline and other models. For ex-

Table 2: Comparison of the MTL models with state-of-the-art on PASCAL-Context dataset. The notation ‘↓’: lower is better. The notation ‘↑’: Higher is better. Δ_m denotes the average per-task performance drop (the higher, the better). Swin- \diamond indicates that the specific Swin model is uncertain. \blacklozenge means we test.

Model	Backbone	SemSeg (mIoU)↑	PartSeg (mIoU)↑	Sal (maxF)↑	Normal (mErr)↓	Bound (odsF)↑	Δ_m [%]↑
single task baseline	HRNet18	62.23	61.66	85.08	13.69	73.06	0.00
multi-task baseline	HRNet18	51.48	57.23	83.43	14.10	69.76	-6.77
PAD-Net (Xu et al., 2018)	HRNet18	53.60	59.60	65.80	15.30	72.50	-4.41
ATRC (Bruggemann et al., 2021)	HRNet18	57.89	57.33	83.77	13.99	69.74	-4.45
MQTransformer(Xu et al., 2022b)	HRNet18	58.91	57.43	83.78	14.17	69.80	-4.20
DeMT (Ours)	HRNet18	59.23	57.93	83.93	14.02	69.80	-3.79
DeMTG (Ours)	HRNet18	59.56	57.71	84.03	14.00	69.70	-3.40
single task baseline	Swin-T	67.81	56.32	82.18	14.81	70.90	0.00
multi-task baseline	Swin-T	64.74	53.25	76.88	15.86	69.00	-3.23
MQTransformer(Xu et al., 2022b)	Swin-T	68.24	57.05	83.40	14.56	71.10	1.07
DeMT (Ours)	Swin-T	69.71	57.18	82.63	14.56	71.20	1.75
DeMTG (Ours)	Swin-T	69.44	58.02	83.31	14.31	71.20	1.94
single task baseline	Swin-S	70.83	59.71	82.64	15.13	71.20	0.00
multi-task baseline	Swin-S	68.10	56.20	80.64	16.09	70.20	-3.97
MQTransformer(Xu et al., 2022b)	Swin-S	71.25	60.11	84.05	14.74	71.80	1.27
DeMT (Ours)	Swin-S	72.01	58.96	83.20	14.57	72.10	1.36
DeMTG (Ours)	Swin-S	71.54	61.49	83.70	14.90	72.20	1.62
single task baseline	Swin-B	74.91	62.13	82.35	14.83	73.30	0.00
multi-task baseline	Swin-B	73.83	60.59	80.75	16.35	71.10	-3.81
MTFormer(Xu et al., 2022a)	Swin- \diamond	74.15	64.89	67.71	-	-	2.41
DeMT (Ours)	Swin-B	75.33	63.11	83.42	14.54	73.20	1.04
DeMTG (3-task) (Ours)	Swin-B	76.77	66.05	83.53	-	-	3.0
DeMTG (Ours)	Swin-B	75.37	64.82	83.75	14.22	73.0	1.84
single task baseline	Swin-L	79.26	68.92	83.84	14.28	74.50	0.00
multi-task baseline	Swin-L	77.35	63.86	82.87	14.84	73.10	-3.33
InvPT(Ye and Xu, 2022)	Swin-L	78.53	68.58	83.71	14.56	73.60	-0.947 \blacklozenge
DeMTG (Ours)	Swin-L	78.54	67.42	83.74	14.17	74.90	-0.38

Table 3: Comparison with MTL models on Cityscapes. We report the results for semantic segmentation (SemSeg) and depth estimation (Depth) tasks. Δ_m denotes the average per-task performance drop (higher is better). ‘↓’: Lower is better. Notation ‘↑’: Higher is better. The best numbers are in **bold**.

Model	SemSeg (mIoU)↑	Depth (aErr)↓	Δ_m [%] (%)↑
STL	75.92	0.0119	0.00
Uncertainty (Kendall et al., 2018)	74.95	0.0121	-1.73
GradNorm (Chen et al., 2018)	74.88	0.0123	-2.70
MGDA (Sener and Koltun, 2018)	75.84	0.0129	-4.65
DWA (Liu et al., 2019)	75.39	0.0121	-1.42
PCGrad (Yu et al., 2020)	75.62	0.0122	-1.73
GradDrop (Chen et al., 2020)	75.69	0.0123	-2.15
IMTL-H (Liu et al., 2021b)	75.33	0.0120	-1.20
CAGrad (Liu et al., 2021a)	75.45	0.0124	-2.69
BAM (Clark et al., 2019)	75.74	0.0122	-1.44
DeMTG (Ours)	77.06	0.0118	1.17

ample, DeMTG improves MQTransformer (Xu et al., 2022b) with the same Swin-T backbone by +1.2 mIoU in SemSeg. Our DeMTG using Swin-T achieves the best performance among models on several metrics and can reach an average per-task performance drop (Δ_m) performance of 1.94 (%). Compared to the MTFormer (Xu et al., 2022a), our DeMTG (3-task) significantly outperforms it on the same three tasks (*i.e.*, Semseg, PartSeg, and Sal). In addition, when using HRNet18 and Swin-

L as the backbone, our DeMTG also achieves the best performance on the Δ_m metric. We also show the dense prediction results in Figure 8 for the PASCAL-Context dataset at 500×375 resolution. DeMTG outperforms InvPT on all datasets. This demonstrates that even using the CNN-based backbone or Transformer-based backbone setting, the DeMTG has the potential to yield further performance gains.

Results on Cityscapes. To further demonstrate the robustness of our method, we also evaluate DeMTG on Cityscapes. We follow the evaluation protocol of prior work (Li et al., 2022b) and report the results in Table 3. In Cityscapes 2-Task, we report the Semseg, depth, and average per-task performance drop. Across all metrics, we find that our DeMTG is significantly better than existing works. We can find that our method continues to achieve consistent and significant improvements (+1.01 (Δ_m)) based on the STL baseline, similar to what we observed for NYUD-v2 and PASCAL-Context datasets.

4.3 MTL Performs Comparable to Unseen Tasks

To analyze the performance of the proposed MTL method on various unseen tasks, we employ the trained model to

Table 4: We report the evaluation results for our DeMTG on NYUD-v2 dataset. Three sets are ' $S-D$ ' (segmentation + depth), ' $S-D-N$ ' (+ normals), and ' $S-D-N-B$ ' (+ boundary). Notation ' \downarrow ': lower is better. Notation ' \uparrow ': Higher is better.

Exp.	Model	Trained	Tested (+ (Task) is on new task)	SemSeg (mIoU) \uparrow	Depth (rmse) \downarrow	Normal (mErr) \downarrow	Bound (odsF) \uparrow
1		Multi-task learning is trained 400 epochs					
1.1	DeMTG	' $S-D$ '	' $S-D$ '	47.98	0.5707	-	-
1.2	DeMTG	' $S-D-N$ '	' $S-D-N$ '	47.07	0.5640	20.00	-
1.3	DeMTG	' $S-D-B$ '	' $S-D-B$ '	47.60	0.5737	-	77.6
1.4	DeMTG	' $S-N-B$ '	' $S-N-B$ '	47.00	-	20.18	77.2
1.5	DeMTG	' $D-N-B$ '	' $D-N-B$ '	-	0.5732	20.04	77.0
1.6	DeMTG	' $S-D-N-B$ '	' $S-D-N-B$ '	47.20	0.5660	20.15	77.2
2		Multi-task learning, adding of task fine-tuning with 100 epochs					
2.1	DeMTG	' $S-D$ '	' $S-D (+N)$ '	47.59	0.5772	21.06	-
2.2	DeMTG	' $S-D$ '	' $S-D (+N, B)$ '	47.47	0.5738	21.01	76.7
2.3	DeMTG	' $S-D-N$ '	' $S-D-N (+B)$ '	46.63	0.5653	19.99	76.6
2.4	DeMTG	' $S-D-N-B$ '	' $S-D-N-B$ '	47.20	0.5660	20.15	77.2
3		Multi-task learning, leave one task out format, addition of the left out task					
3.1	DeMTG	' $S-D-N$ '	' $S-D-N (+B)$ '	46.72	0.5671	20.12	29.3
3.2	DeMTG	' $S-D-B$ '	' $S-D-B (+N)$ '	47.03	0.5717	100.66	22.5
3.3	DeMTG	' $S-N-B$ '	' $S-N-B (+D)$ '	46.72	3.0126	47.42	21.2
3.4	DeMTG	' $D-N-B$ '	' $D-N-B (+S)$ '	0.475	2.2626	50.26	14.0

evaluate the effect of adding the new tasks on NYUD-v2 dataset, as shown in Table 4. We design various settings which can be divided into two categories: augmenting tasks (Exp. 1 and 2) and leave one out (Exp. 3). Specifically, we fine-tuned all Exp. 2 experiments for 100 epochs. In Exp. 3, we leverage the leave-one-task-out trained MTL model to evaluate the all task (*i.e.*, *four tasks*) on NYUD-v2 dataset.

The effects of unseen task fine-tuning. In Table 4, ' $+ Task$ ' denotes that the model is first trained on a set of tasks and then further fine-tuning on the new task. This approach is considered as adding a new task to the multi-task architecture, where the model learns to adapt and improve its performance on the newly introduced task during the fine-tuning process. The Exp. 1 and 2 (all variants), in Table 4 indicate the DeMTG exhibits a strong adding new task performance. For example, Exp. 2.3 with only 100 epochs of fine-tuning on the *Boundary* task, the model achieves an odsF of 76.6% on the NYUD-v2. This illustrates the successful adaptation of our approach to new tasks within a limited training duration. In addition, we also observe that training all the tasks together in a multi-task setting (*i.e.*, Exp. 2.4) is better than fine-tuning some tasks (*i.e.*, Exp. 2.1, 2.2, and 2.3). We conclude that fine-tuning on different adding new task can achieve the competitive performance with 1/4 training epochs, allowing for better generalization.

Evaluate new tasks using the trained model. As shown in Exp. 3 of Table 4, we employ the leave-one-task-out trained model to directly evaluate the tasks that were left out during training. We further report the leave one task out format results (*i.e.*, Exp. 3.1,

3.2, 3.3, and 3.4). We can see that the performance of adding of the left out task exhibits very weak results (see the **orange numbers** in Exp. 3). Specifically, the ' $S-N-B$ ' (Exp. 3.3) model degrades in performance on the depth, normal, and boundary tasks, but remains competitive on the segmentation task. It is worth noting that the ' $D-N-B$ ' (Exp. 3.4) model does not learn the semantic segmentation feature, resulting in a significant performance degradation for all tasks. These results demonstrate that semantic segmentation features play an essential role. Exp. 3 provides information on the effect of the interactions between task pairs on model performance, which helps further understand the contribution of tasks in MTL.

4.4 Ablation Studies

We carry out ablations using Swin-T on the NYUD-v2 dataset. We ablate DeMTG to understand the individual contribution of each component and settings. This analysis allows us to gain insights into the importance and effectiveness of each part in the overall performance of our method.

Ablation on modules. We analyze the influence of every key component and design choice in our full method. All models are trained for 400 epochs on NYUD-v2. The DeMTG model consists of three components: deformable mixer, task interaction, and task query gating blocks. As shown in Table 5(a), we demonstrate the advantages of the deformable mixer, task interaction, and task query gating blocks. After adding the proposed blocks to the multi-task baseline (MTB) network, the results improved persistently and notably. Specifically,

Table 5: Ablation studies and analysis on NYUD-v2 dataset using a Swin-T backbone. Deformable mixer (DM), task interaction (TI) block, and task query gating (TQG) block are the parts of our model. The Shared spatial gating (SSG) layer inserts into the TQG block. HR48 denotes HRNet48. MTB denotes the multi-task baseline. The notation ‘↓’: lower is better. The notation ‘↑’: Higher is better. The w/ indicates ”with”.

(a) Ablation on components					(b) Ablation on the depths (d) of DM encoder				
Model	SemSeg (mIoU)↑	Depth (rmse)↓	Normal (mErr)↓	Bound (odsF)↑	d	SemSeg (mIoU)↑	Depth (rmse)↓	Normal (mErr)↓	Bound (odsF)↑
MTB	38.78	0.6312	21.05	75.6	1	46.96	0.5717	20.22	77.1
w/ DM	42.40	0.6069	20.83	76.2	2	47.20	0.5660	20.15	77.2
w/ DM+TI	44.44	0.5969	20.75	76.4	4	48.12	0.5601	20.01	77.3
DeMT	46.36	0.5871	20.65	76.9	8	48.01	0.5521	19.81	77.2
DeMT+SSG	47.20	0.5660	20.15	77.2					
Gain vs DeMT	+0.84	+0.0211	+0.5	+0.3					

(c) Ablation on scales					(d) Ablation on backbones				
Scale	SemSeg (mIoU)↑	Depth (rmse)↓	Normal (mErr)↓	Bound (odsF)↑	Backbone	SemSeg (mIoU)↑	Depth (rmse)↓	Normal (mErr)↓	Bound (odsF)↑
1/4	6.81	1.0851	31.65	66.5	HR48 baseline	41.96	0.5543	20.36	77.6
1/4, 1/8	16.91	0.8133	27.06	71.2	HR48 w/ ours	46.87	0.5409	20.10	77.8
1/4, 1/8, 1/16	41.32	0.6254	21.18	76.8	Swin-B baseline	51.44	0.5813	20.44	78.0
1/4,1/8,1/16,1/32	47.20	0.5660	20.15	77.2	Swin-B+InvPT	50.97	0.5071	19.39	77.3
					Swin-B w/ ours	54.45	0.5228	19.33	78.6

we observe that the task interaction block has more effect on the performance, and it is essential to interact with the whole task features for task interaction information. This indicates that task interaction and task query gating blocks are essential to the task-aware gating transformer decoder. From Figure 8 and Table 5(a) it can be observed that different components play a beneficial role.

Effectiveness of shared spatial gating (SSG). Further, we conduct an ablation study on the gating mechanism in our task query gating block. We design a shared spatial gating across all task query gating blocks. As shown in Table 5(a), the inclusion of shared spatial gating (SSG) layer into our task-aware gating transformer decoder provides a performance boost of around +8.86 mIoU (ours: 47.46 v.s MTB: 38.78) and +0.0615 rmse (ours: 0.5697 v.s MTB: 0.6312), which supports the effectiveness of the proposed SSG in selecting task awareness features. We observe that the task query gating block equipped with shared spatial gating can obtain higher performance than the original framework. This demonstrates the benefits shared spatial gating layer among different tasks. To further highlight the ability of task query gating block, we visualize the dense predictions as shown in Figure 8. We observe that DeMTG significantly boosts the performance over the original DeMT (from 46.36 mIoU to 47.46 mIoU on the SemSeg task, from 0.5871 rmse to 0.569 rmse on the Depth task). It clearly proves that our method benefits from

the efficient use of shared spatial gating to insert the task query gating block.

Ablation on the depths d . As shown in Figure 4, the depth d is the number of repetitions of the deformable mixer. We add the d to analyze the effect of the depth of the deformable mixer on the DeMT model. In Table 5(b), We vary the number of used deformable mixer depths (*e.g.*, 1, 2, 4, 8) and compare their performances. Comparing the first to last row in Table 5(b), we observe the best performance when the depth is set to 4. However, as increasing the depth, the parameters and GFLOPs also become more extensive. Practically, we choose a depth $d = 1$ for all models in this paper.

Ablation on scales. We explore the influence of using different scale features. In Figure 3, the backbone outputs four-scale (1/4, 1/8, 1/16, 1/32) features. Table 5(c) shows the influence of using a different number of scales. Note that the model performance increases obviously with the increasing number of scales. We observe that our model performs very poorly when using only 1/4 scale features as input. This highlights the importance of incorporating features from multiple scales to improve the performance. Our method can capture valuable semantic information for multiple tasks. Practically, we choose four-scale features for all models.

Ablation on backbones. Table 5(d) shows the results using the different backbones (*i.e.*, HRNet48 and Swin-B). To deeper explore the capacity of our DeMTG, we employ extensive backbones to conduct the ablation experiment. It is worth noting that our DeMTG

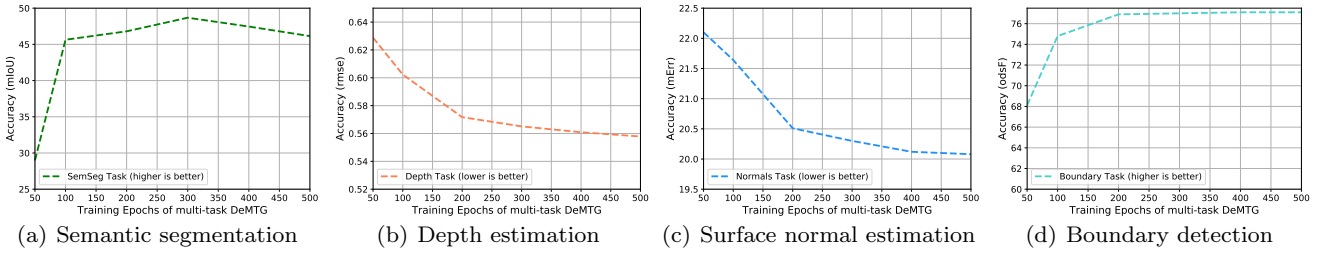


Fig. 6: Influence of the number of epochs in multi-task training using Swin-T backbone on NYUD-v2. To evaluate the DeMTG performance of different epochs, we pick out models at the 50th, 100th, 200th, 300th, 400th and 500th epoch.

Table 6: Ablation on shared spatial gating depth (d) in task query gating. The best numbers are in **bold**.

d	SemSeg (mIoU) \uparrow	Depth (rmse) \downarrow	Normals (mErr) \downarrow	Bound (odsF) \uparrow
1	47.20	0.5660	20.15	77.2
2	47.33	0.5611	20.12	77.1
4	47.55	0.5646	20.12	77.3
6	47.29	0.5621	20.05	77.5
8	47.45	0.5587	20.05	77.6

Table 7: Ablation on attention head numbers using Swin-T backbone on NYUD-v2. The best numbers are in **bold**.

Head Number	SemSeg (mIoU) \uparrow	Depth (rmse) \downarrow	Normals (mErr) \downarrow	Bound (odsF) \uparrow
2	47.59	0.5622	20.11	77.2
4	47.20	0.5660	20.15	77.2
16	47.20	0.5652	20.12	77.1
32	47.16	0.5598	20.11	77.0
64	47.11	0.5643	20.49	77.0

leads to the best performance on all metrics when using Swin-B on NYUD-v2. As reported in Table 5(d) and Figure 1, the proposed DeMTG using Swin-B provides +3.82 mIoU (SemSeg) improvement over the existing competitive InvPT (Ye and Xu, 2022), which requires $4.3\times$ (Our parameters: 93.1M *v.s.* InvPT: 402.1M) more parameters compared to DeMTG. In addition, we also observe the inspiring fact that using a larger transformer backbone can easily reach top-tier performance. The different backbones are compared to demonstrate the generalization of our method.

Ablation on the depths (d) of shared spatial gating in task query gating block. We conduct an ablation study to evaluate the effect of the depth of the shared spatial gating in task query gating block. We set the shared spatial gating depth number $\{1, 2, 4, 6, 8\}$ in Table 6. Using several depths shows a slight performance gain, and at a cost of significantly more parameters. In other experiments, the depth of shared spatial gating for model training is set to 1 by default.

Effectiveness of attention head numbers. The attention head numbers are set in the task interaction and task query gating blocks. As shown in Table 7, we set the attention head number $\{2, 4, 16, 32, 64\}$. We compare the effect of the number of attention head numbers. We find that having a larger attention head number improves the performance slightly, whereas increasing the number of attention heads does not improve the whole MTL performance. In other experiments, the number of attention for model training is set to 4 by default.

Ablation on different epochs. Further, we conduct the ablation on different epochs to evaluate the DeMTG performance of different epochs. As shown in Figure 6, we train our DeMTG using Swin-T as the backbone on NYUD-v2 dataset. We pick out models at the 50th, 100th, 200th, 300th, 400th and 500th epochs. Figure 6 shows two interesting pieces of information. 1) Increasing the number of training epochs can improve task performance up to a certain point, after which further training can lead to over-fitting and degrade performance on the test set. 2) The optimal number of training epochs depends on factors such as task relatedness. Figure 6 (a) shows that the semantic segmentation (SemSeg) task starts to decrease as the number of training epochs increases beyond 300. Figure 6 (b), (c), and (d) show a continuous increase in accuracy for these tasks as the number of training epochs increases. Proper hyper-parameter tuning is important for achieving optimal performance on all tasks while avoiding over-fitting.

4.5 Visualization

To deeper understand our DeMTG model, we visualize the multiple task predictions. As shown in Figure 8 and 7, we show the qualitative results in different dimensions. Figure 8 showcases the impact of our approach using different components: while only the Baseline + DM (deformable mixer encoder) fails to visual-

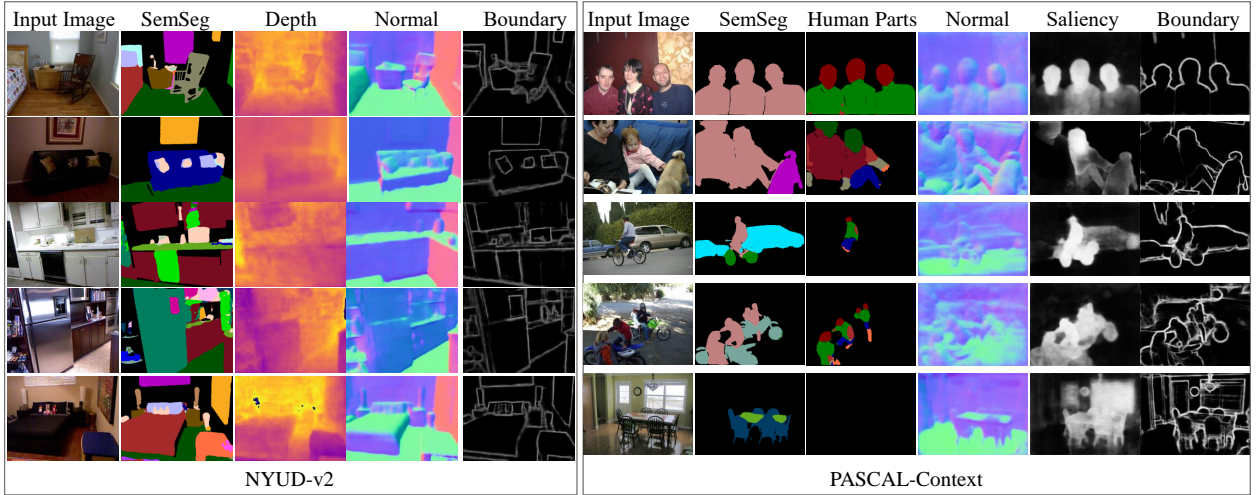


Fig. 7: The left of the visualization illustrates five examples from the NYUD-v2 dataset. The right of the visualization illustrates five examples from the PASCAL-Context dataset. Best viewed in color and zoom.

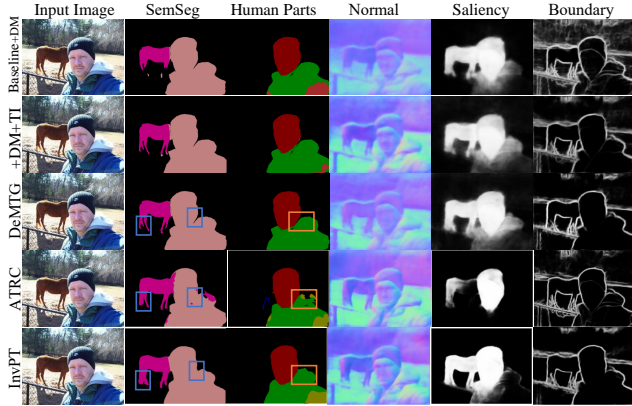


Fig. 8: Visual results on 5-task PASCAL-Context dataset. Qualitative analysis of the components according to Table 5(a). We also select the visualization results of ATRC (Bruggemann et al., 2021) and InvPT (Ye and Xu, 2022) as a comparison. Note that they are marked in blue and orange square boxes. The qualitative comparison clearly proves the efficacy of our model in capturing the objects’ subtle contextual details. Best viewed in color and zoom.

ize some objects, the second row shows DeMTG’s improvements to multiple task predictions. Note that we not only report these results for qualitative understanding of the model but also evaluate it quantitatively in Table 5(a). We compared the prediction results of the DeMTG model with the ATRC (Bruggemann et al., 2021)(Figure 8 next-to-last row), and our results are significantly better than ATRC, especially on semantic segmentation and human parts segmentation tasks on PASCAL-Context. We also provide the visualizations of InvPT (Ye and Xu, 2022) in Figure 8 last row. When InvPT (Ye and Xu, 2022) fails to yield a satisfactory prediction on the SemSeg task, as shown in marked blue

boxes, our MeMTG can perform a good prediction (See Figure 8). Overall, similar to the quantitative results, it is evident from the qualitative results that DeMTG outperforms the competitive methods for all tasks.

Figure 7 shows the capability of DeMTG with Swin-S backbone to perform dense predictions with strong expressive power and successfully capture the task-specific features on NYUD-v2 and PASCAL-Context. As illustrated in Figure 7 (Right), the second and third columns focus mainly on specific semantics such as human, animal, and other objects on the PASCAL-Context. It is also easy to notice that our DeMTG model produces higher-quality predictions than both the Transformer-based baseline and CNN-based MTL models.

5 Conclusion

In this work, we introduce the DeMTG, a simple and effective approach that leverages the combination of both merits of deformable CNN and query-based Transformer with gating for multi-task learning of dense prediction. Significantly, the deformed feature produced by the deformable mixer encoder is leveraged as a task query in the task-aware gating transformer decoder by query-base attention with a gating mechanism to disentangle task-specific features. Extensive experiments conducted on three popular MTL datasets for dense prediction tasks, namely NYUD-v2, PASCAL-Context, and Cityscapes, demonstrate the effectiveness of our proposed DeMTG model.

Limitations and future work. Though DeMTG performs well in general, it is not perfect. DeMTG only uses a naive operation to aggregate multi-scale features

and could be further improved in two aspects: 1) Consider using the FPN or FPN variant to aggregate multi-scale features. 2) Design a flexible training strategy to balance training tasks.

Data Availability

The datasets generated and/or analysed during the current study are available in the NYUD-v2, PASCAL-Context, and Cityscapes repositories, https://cs.nyu.edu/~silberman/datasets/nyu_depth_v2.html, <https://www.cs.stanford.edu/~roozbeh/pascal-context/>, and <https://www.cityscapes-dataset.com/>.

References

- Bhattacharjee D, Zhang T, Süssstrunk S, Salzmann M (2022) Mult: An end-to-end multitask learning transformer. In: CVPR, pp 12031–12041
- Bruggemann D, Kanakis M, Obukhov A, Georgoulis S, Gool LV (2021) Exploring relational context for multi-task dense prediction. In: ICCV, pp 15869–15878
- Carion N, Massa F, Synnaeve G, Usunier N, Kirillov A, Zagoruyko S (2020) End-to-end object detection with transformers. In: ECCV, pp 213–229
- Chen X, Mottaghi R, Liu X, Fidler S, Urtasun R, Yuille A (2014) Detect what you can: Detecting and representing objects using holistic models and body parts. In: CVPR, pp 1971–1978
- Chen Z, Badrinarayanan V, Lee CY, Rabinovich A (2018) GradNorm: Gradient normalization for adaptive loss balancing in deep multitask networks. In: ICML, pp 794–803
- Chen Z, Ngiam J, Huang Y, Luong T, Kretzschmar H, Chai Y, Anguelov D (2020) Just pick a sign: Optimizing deep multitask models with gradient sign dropout. *NeurIPS* 33:1–12
- Chen Z, Duan Y, Wang W, He J, Lu T, Dai J, Qiao Y (2023) Vision transformer adapter for dense predictions. In: ICLR
- Clark K, Luong MT, Khandelwal U, Manning CD, Le QV (2019) Bam! born-again multi-task networks for natural language understanding. In: ACL, pp 5931–5937
- Cordts M, Omran M, Ramos S, Rehfeld T, Enzweiler M, Benenson R, Franke U, Roth S, Schiele B (2016) The cityscapes dataset for semantic urban scene understanding. In: CVPR, pp 3213–3223
- Dai J, Qi H, Xiong Y, Li Y, Zhang G, Hu H, Wei Y (2017) Deformable convolutional networks. In: ICCV, pp 764–773
- Dauphin YN, Fan A, Auli M, Grangier D (2017) Language modeling with gated convolutional networks. In: ICML, pp 933–941
- Dong X, Bao J, Chen D, Zhang W, Yu N, Yuan L, Chen D, Guo B (2022) Cswin transformer: A general vision transformer backbone with cross-shaped windows. In: CVPR, pp 12124–12134
- Dosovitskiy A, Beyer L, Kolesnikov A, Weissenborn D, Zhai X, Unterthiner T, Dehghani M, Minderer M, Heigold G, Gelly S, Uszkoreit J, Houlsby N (2021) An image is worth 16x16 words: Transformers for image recognition at scale. In: ICLR
- Fei Z (2022) Attention-aligned transformer for image captioning. In: AAAI, vol 36, pp 607–615
- Gao Y, Ma J, Zhao M, Liu W, Yuille AL (2019) Nddr-cnn: Layerwise feature fusing in multi-task cnns by neural discriminative dimensionality reduction. In: CVPR, pp 3205–3214
- Ghiasi G, Zoph B, Cubuk ED, Le QV, Lin TY (2021) Multi-task self-training for learning general representations. In: ICCV, pp 8856–8865
- Jaegle A, Gimeno F, Brock A, Vinyals O, Zisserman A, Carreira J (2021) Perceiver: General perception with iterative attention. In: ICML, pp 4651–4664
- Kendall A, Gal Y, Cipolla R (2018) Multi-task learning using uncertainty to weigh losses for scene geometry and semantics. In: CVPR, pp 7482–7491
- Kokkinos I (2017) Ubernet: Training a universal convolutional neural network for low-, mid-, and high-level vision using diverse datasets and limited memory. In: CVPR, pp 6129–6138
- Lan M, Zhang J, He F, Zhang L (2022) Siamese network with interactive transformer for video object segmentation. In: AAAI, pp 1228–1236
- Li WH, Liu X, Bilen H (2022a) Learning multiple dense prediction tasks from partially annotated data. In: CVPR, pp 18879–18889
- Li WH, Liu X, Bilen H (2022b) Universal representations: A unified look at multiple task and domain learning. *arXiv preprint arXiv:220402744*
- Ling Z, Zhen C, Chunyan X, Zhenyu Z, Chaoqun W, Tong Z, Jian Y (2020) Pattern-structure diffusion for multi-task learning. In: CVPR, pp 4514–4523
- Liu B, Liu X, Jin X, Stone P, Liu Q (2021a) Conflict-averse gradient descent for multi-task learning. In: *NeurIPS*, pp 18878–18890
- Liu L, Li Y, Kuang Z, Xue J, Chen Y, Yang W, Liao Q, Zhang W (2021b) Towards impartial multi-task learning. In: ICLR
- Liu S, Johns E, Davison AJ (2019) End-to-end multi-task learning with attention. In: CVPR, pp 1871–1880

- Liu Z, Lin Y, Cao Y, Hu H, Wei Y, Zhang Z, Lin S, Guo B (2021c) Swin transformer: Hierarchical vision transformer using shifted windows. In: ICCV, pp 10012–10022
- Misra I, Shrivastava A, Gupta A, Hebert M (2016) Cross-stitch networks for multi-task learning. In: CVPR, pp 3994–4003
- Ranftl R, Bochkovskiy A, Koltun V (2021) Vision transformers for dense prediction. In: CVPR, pp 12179–12188
- Rao Y, Zhao W, Tang Y, Zhou J, Lim SN, Lu J (2022) HorNet: Efficient high-order spatial interactions with recursive gated convolutions. In: NeurIPS, vol 35, pp 10353–10366
- Ru L, Zhan Y, Yu B, Du B (2022) Learning affinity from attention: End-to-end weakly-supervised semantic segmentation with transformers. In: CVPR, pp 16846–16855
- Sener O, Koltun V (2018) Multi-task learning as multi-objective optimization. In: NeurIPS, pp 525–536
- Silberman N, Hoiem D, Kohli P, Fergus R (2012) Indoor segmentation and support inference from rgbd images. In: ECCV, pp 746–760
- Sun K, Xiao B, Liu D, Wang J (2019) Deep high-resolution representation learning for human pose estimation. In: CVPR, pp 5693–5703
- Vandenhende S, Georgoulis S, Van Gool L, Van Gool L (2020) Mti-net: Multi-scale task interaction networks for multi-task learning. In: ECCV, pp 527–543
- Vandenhende S, Georgoulis S, Gansbeke WV, Proesmans M, Dai D, Gool LV (2021) Multi-task learning for dense prediction tasks: A survey. *IEEE TPAMI* 44(7):3614–3633
- Vaswani A, Shazeer N, Parmar N, Uszkoreit J, Jones L, Gomez AN, Kaiser Ł, Polosukhin I (2017) Attention is all you need. *NeurIPS*
- Wang W, Xie E, Li X, Fan DP, Song K, Liang D, Lu T, Luo P, Shao L (2021) Pyramid vision transformer: A versatile backbone for dense prediction without convolutions. In: ICCV, pp 568–578
- Xia Z, Pan X, Song S, Li LE, Huang G (2022) Vision transformer with deformable attention. In: CVPR, pp 4794–4803
- Xu D, Ouyang W, Wang X, Sebe N (2018) Pad-net: Multi-tasks guided prediction-and-distillation network for simultaneous depth estimation and scene parsing. In: CVPR, pp 675–684
- Xu X, Zhao H, Vineet V, Lim SN, Torralba A (2022a) MTFormer: Multi-task learning via transformer and cross-task reasoning. In: ECCV, pp 304–321
- Xu Y, Li X, Yuan H, Yang Y, Zhang L (2022b) Multi-task learning with multi-query transformer for dense prediction. *arXiv preprint arXiv:220514354*
- Xu Y, Yang Y, Zhang L (2023) DeMT: Deformable mixer transformer for multi-task learning of dense prediction. In: AAAI, vol 37, pp 3072–3080
- Yang J, Li C, Dai X, Gao J (2022) Focal modulation networks. In: NeurIPS, vol 35, pp 4203–4217
- Yang Y, Li H, Li X, Zhao Q, Wu J, Lin Z (2020) SogNet: Scene overlap graph network for panoptic segmentation. In: AAAI, vol 34, pp 12637–12644
- Ye H, Xu D (2022) Inverted pyramid multi-task transformer for dense scene understanding. In: ECCV, pp 514–530
- Yu T, Kumar S, Gupta A, Levine S, Hausman K, Finn C (2020) Gradient surgery for multi-task learning. In: NeurIPS, vol 33, pp 5824–5836
- Zhang Z, Cui Z, Xu C, Yan Y, Sebe N, Yang J (2019) Pattern-affinitive propagation across depth, surface normal and semantic segmentation. In: CVPR, pp 4106–4115
- Zhu X, Hu H, Lin S, Dai J (2019) Deformable convnets v2: More deformable, better results. In: CVPR, pp 9308–9316
- Zhu X, Su W, Lu L, Li B, Wang X, Dai J (2021) Deformable DETR: deformable transformers for end-to-end object detection. In: ICLR